

A three-dimensional exact state-space solution for cylindrical bending of continuously non-homogenous piezoelectric laminated plates with arbitrary gradient composition

M. LEZGY-NAZARGAH

*Faculty of Civil Engineering
Hakim Sabzevari University
Sabzevar, Iran
e-mail: m.lezgy@hsu.ac.ir*

MOST OF EXACT SOLUTIONS REPORTED FOR the analysis of functionally graded piezoelectric (FGP) plates are based on the assumption, that the graded plate consists of a number of layers, where the material properties within each layer are invariant. The limited works that consider the continuous variation of electro-mechanical properties are restricted to FGP materials with the exponent-law dependence on the thickness-coordinate. In the present paper, a three-dimensional (3D) exact solution is presented for cylindrical bending of the FGP laminated plates based on the state space formalism. In contrast to the other reported solutions which are restricted to FGP materials with the exponent-law dependence on the thickness-coordinate, the present exact solution considers materials with arbitrary compositional gradient. Moreover, no assumption on displacement components and the electric potential along the thickness direction of FGP layers is introduced. Regardless of the number of layers, equations of motion, charge equation, and the boundary and interface conditions are satisfied exactly. The obtained exact solution can be used to assess the accuracy of different FGP laminated plate theories and/or for validating finite element codes.

Key words: exact solution, state-space approach, functionally graded piezoelectric materials, laminated plate.

Copyright © 2015 by IPPT PAN

1. Introduction

PIEZOELECTRIC MATERIALS HAVE FOUND MANY APPLICATION as sensors and actuators for the purpose of monitoring and controlling the response of intelligent structures due to their coupled mechanical and electrical properties. Accurate simulation and theoretical modelling of intelligent structures have been intensive areas of research for more than two decades. Various mathematical models have been presented for laminated composite structures with piezoelectric sensors and actuators until now [1–12].

In order to achieve large deformations, the piezoelectric actuators are often made of several layers of different piezoelectric materials. Although this conventional type of design may provide larger deformations, it has several restricting

disadvantages that reduce its reliability. For the piezoelectric actuators made of different piezoelectric layers or identical piezoelectric layers with different poling directions, high stress concentrations usually appear at the layer interfaces under mechanical or electrical loading. These stress concentrations lead to the initiation and propagation of micro-cracks near the interfaces of two bonded piezoelectric layers. Such drawbacks reduce lifetime and reliability of these structures.

To reduce the limitations of the conventional piezoelectric laminates, sensors and actuators with graded properties were introduced and fabricated by ZHU and MENG [13], and WU *et al.* [14]. A functionally graded piezoelectric is a kind of piezoelectric materials whose mechanical and electrical properties vary continuously in one or more directions. Functionally graded piezoelectric actuators not only can produce large displacements but also reduce the internal stress concentrations and consequently significantly improve the lifetime of piezoelectric actuators. It is obvious that functionally graded sensors and actuators will have a significant function in the field of smart materials and structures.

Several researches have dealt in recent years with the static and dynamic responses of FGP structures, such as beams, plates and shells. Most of these studies are based on various beam and plate/shell theories. In early works on the structural analysis of FGP structures, it was assumed that the FGP layer consists of a number of sub-layers, where the material properties within each sub-layer are invariant. The accuracy of these methods not only is dependent on the number of sub-layers but also leads to inaccurate results in the prediction of responses of thick FGP actuators. Liu and TANI [15] used this method to study the wave propagation in FGP plates. CHEN and DING [16] analyzed the free vibration of FGP rectangular plates using the aforementioned method. LEE [17] used a layer-wise finite element formulation to investigate the displacement and stress response of an FGP bimorph actuator. Using the state-space and differential quadrature method (DQM), LI and SHI [18] investigated the free vibration of an FGP beam. By using the Timoshenko beam theory, YANG and XIANG [19] investigated the static and dynamic response of FGP actuators under thermo-electro-mechanical loadings. In their work, the numerical results were obtained by using the DQM. A comprehensive study on the static, dynamic and free vibration response of FGP panels under different sets of mechanical, thermal and electrical loadings using the finite element method was presented by BEHJAT *et al.* [20]. BEHJAT *et al.* [21] investigated also the static bending, free vibration and dynamic response of FGP plates under mechanical and electrical loads using the first-order shear deformation theory. WU *et al.* [22] derived a high-order theory for FGP shells based on generalized Hamilton's principle. The performance of an FGP monomorph in static and dynamic states was investigated by LI *et al.* [23] using the electrophoretic deposition. LIU and SHI [24], and SHI and CHEN [25] obtained closed form solutions for the FGP cantilever beams using the

two-dimensional (2D) theory of elasticity and the Airy stress function. XIANG and SHI [26] investigated thermo-electro-elastic response of an FGP sandwich cantilever. They employed also the Airy stress function in order to study the effect of parameters such as the electromechanical coupling, functionally graded index, temperature change and thickness ratio on the static behavior of actuators/sensors. LEZGY-NAZARGAH *et al.* [27] proposed an efficient finite element model for static and dynamic analyses of FGP beams. They used an efficient three-nodded beam element which is based on a refined sinus model. The proposed beam element of these researchers does not require shear correction factor and ensures continuity conditions for displacements, transverse shear stresses as well as boundary conditions on the upper and lower surfaces of the FGP beam. LEZGY-NAZARGAH and FARAHBAKHS [28] investigated the relation between the material gradient properties and the optimum sensing/actuation design of the FGP beams. They employed 3D finite element analysis for the prediction of an optimum composition profile in these types of sensors and actuators. By using the refined 2D models, BRISCHETTO and CARRERA [29] studied the static response of a single-layered FGP plate. In this work, Carrera's unified formulation has been extended to FGP plates in the framework of the principle of virtual displacements.

To assess the validity of approximate theories related to FGP structures, obtaining 3D analytical solutions based on the exact theory of piezoelectricity is necessary. LIM and HE [30] obtained the exact solution for a compositionally graded piezoelectric layer under uniform stretch, bending and twisting. By dividing the FGP layer into a number of homogenous sub-layers, REDDY and CHENG [31] obtained a 3D solution for smart functionally gradient plates. ZHONG and SHANG [32] presented the exact 3D solution for rectangular piezoelectric plates with exponent-law dependency of electromechanical properties on the thickness-coordinate by means of the state space approach. LU *et al.* [33] presented the exact solution for simply supported exponentially non-homogenous piezoelectric laminates in cylindrical bending by Stroh-like formalism. Using this method, LU *et al.* [34] also proposed the exact solutions for simply supported FGP plates.

Nowadays, the design and fabrication of materials with arbitrary compositional gradient is possible by means of the modern materials processing technology. To the best knowledge of author, there is no exact solution in the literature for the accurate analysis of FGP laminates with arbitrary compositional gradient. In this paper an exact solutions for cylindrical bending of FGP laminates with arbitrary gradient composition is derived based on the state space approach without a priori assumptions on displacement fields, electric potential and stress fields. The obtained solution is exact in that the electric potential, displacements and stresses satisfy exactly the governing equations of anisotropic

piezoelectricity, the traction boundary conditions on the top and bottom planes, the end conditions as well as the interlaminar continuity conditions on the interfaces between the layers, regardless of the number of layers. In contrast to the reference [33] which assumes an exponential-law for the variation of the mechanical and electrical properties along the thickness direction, the present obtained exact solution is general and considers piezoelectric materials with arbitrary compositional gradient. Moreover, the exact solution obtained in the present study is very concise, simple in concept and systematic in operation. In order to assess the accuracy of the present state-space formulation, comparisons have been made with other results available in the literature. The numerical results obtained from the present formulation exhibit excellent agreements with other published results.

2. Formulation of the problem

The considered laminated plate is a prismatic one with a rectangular uniform cross section of length L , height h and made of N_l layers either completely or in part from FGP materials. The laminate is assumed to be infinitely long in the x_2 -direction, with perfect bonding between layers. The geometric parameters of the laminated plate and the chosen Cartesian coordinate system (x_1, x_2, x_3) are shown in Fig. 1.

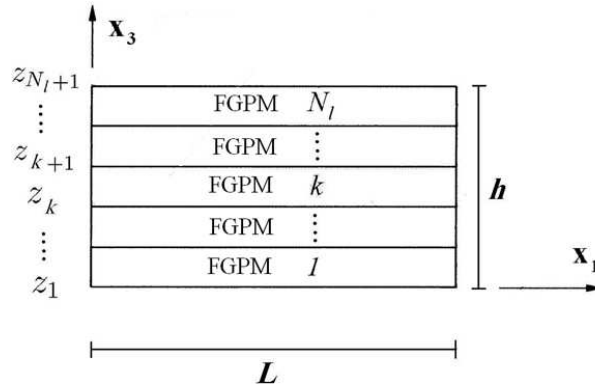


FIG. 1. Functionally graded piezoelectric plate in cylindrical bending: Cartesian coordinate system and geometric parameters.

In this study, the general type of piezoelectric materials is assumed to be “monoclinic class 2”. Thus, the 3D linear constitutive equations of the k th layer, polarized along its thickness direction in its global material coordinate system can be expressed as:

(2.1)

$$\begin{aligned}
\begin{Bmatrix} \sigma_{11} \\ \sigma_{22} \\ \sigma_{33} \\ \sigma_{23} \\ \sigma_{13} \\ \sigma_{12} \end{Bmatrix}^{(k)} &= \begin{bmatrix} c_{11}(x_3) & c_{12}(x_3) & c_{13}(x_3) & 0 & 0 & c_{16}(x_3) \\ c_{12}(x_3) & c_{22}(x_3) & c_{23}(x_3) & 0 & 0 & c_{26}(x_3) \\ c_{13}(x_3) & c_{23}(x_3) & c_{33}(x_3) & 0 & 0 & c_{36}(x_3) \\ 0 & 0 & 0 & c_{44}(x_3) & c_{45}(x_3) & 0 \\ 0 & 0 & 0 & c_{45}(x_3) & c_{55}(x_3) & 0 \\ c_{16}(x_3) & c_{26}(x_3) & c_{36}(x_3) & 0 & 0 & c_{66}(x_3) \end{bmatrix}^{(k)} \begin{Bmatrix} \varepsilon_{11} \\ \varepsilon_{22} \\ \varepsilon_{33} \\ 2\varepsilon_{23} \\ 2\varepsilon_{13} \\ 2\varepsilon_{12} \end{Bmatrix}^{(k)} \\
&\quad - \begin{bmatrix} 0 & 0 & e_{31}(x_3) \\ 0 & 0 & e_{32}(x_3) \\ 0 & 0 & e_{33}(x_3) \\ e_{14}(x_3) & e_{24}(x_3) & 0 \\ e_{15}(x_3) & e_{25}(x_3) & 0 \\ 0 & 0 & e_{36}(x_3) \end{bmatrix}^{(k)} \begin{Bmatrix} E_1 \\ E_2 \\ E_3 \end{Bmatrix}^{(k)}, \\
\begin{Bmatrix} D_1 \\ D_2 \\ D_3 \end{Bmatrix}^{(k)} &= \begin{bmatrix} 0 & 0 & 0 & e_{14}(x_3) & e_{15}(x_3) & 0 \\ 0 & 0 & 0 & e_{24}(x_3) & e_{25}(x_3) & 0 \\ e_{31}(x_3) & e_{32}(x_3) & e_{33}(x_3) & 0 & 0 & e_{36} \end{bmatrix}^{(k)} \begin{Bmatrix} \varepsilon_{11} \\ \varepsilon_{22} \\ \varepsilon_{33} \\ 2\varepsilon_{23} \\ 2\varepsilon_{13} \\ 2\varepsilon_{12} \end{Bmatrix}^{(k)} \\
&\quad + \begin{bmatrix} \chi_{11}(x_3) & \chi_{12}(x_3) & 0 \\ \chi_{12}(x_3) & \chi_{22}(x_3) & 0 \\ 0 & 0 & \chi_{33}(x_3) \end{bmatrix}^{(k)} \begin{Bmatrix} E_1 \\ E_2 \\ E_3 \end{Bmatrix}^{(k)},
\end{aligned}$$

where σ_{ij} , ε_{ij} and E_i denote the stress tensor, the infinitesimal strain tensor and the electric field components respectively. D_i is the electric displacement vector components and c_{kl} , e_{ik} , χ_{ij} elastic, piezoelectric and dielectric material constants. Unlike the homogeneous piezoelectric materials, c_{kl} , e_{ik} and χ_{ij} are now functions of the coordinate x_3 . They may vary according to the power-law, exponent-law or every other arbitrary distribution along the thickness direction of FGP layers. Indeed, the anisotropy of the considered laminated FGP plate medium of the present study belongs to the monoclinic class 2 with the symmetry axis 2 orthogonal to the layers. It is worthy to note that the similar studies available in the literature only consider the FGP materials with the exponent-law dependence on the thickness-coordinate.

The displacement components u_i are related to the strain components through the relations

$$(2.2) \quad \varepsilon_{ij}^{(k)} = \frac{1}{2}(u_{i,j}^{(k)} + u_{j,i}^{(k)}).$$

The electric field components can be related to the electrostatic potential φ using

the relation

$$(2.3) \quad E_i^{(k)} = -\varphi_{,i}^{(k)}.$$

The equilibrium equations in the absence of body forces and free charges for the k th lamina made of a piezoelectric material are

$$(2.4) \quad \sigma_{ij,j}^{(k)} = 0, \quad D_{i,i}^{(k)} = 0.$$

In cylindrical bending, the laminate is simply supported and the vertical edges are assumed to be grounded. These conditions can be expressed as:

$$(2.5) \quad \sigma_{11}^{(k)}(0, x_3) = \sigma_{11}^{(k)}(L, x_3) = 0, \quad \sigma_{12}^{(k)}(0, x_3) = \sigma_{12}^{(k)}(L, x_3) = 0,$$

$$(2.6) \quad u_3^{(k)}(0, x_3) = u_3^{(k)}(L, x_3) = 0, \quad \varphi^{(k)}(0, x_3) = \varphi^{(k)}(L, x_3) = 0.$$

Although the electric potential does not vanish at the boundaries, exact 3D solutions for laminated plates can be obtained only for certain combinations of boundary conditions on the edges. In other words, we are able to obtain exact solutions only when the vertical edges of the laminated plate are assumed to be electrically grounded. HEYLIGER and BROOKS [35] have also employed the same assumption in order to obtain exact solutions for the cylindrical bending of laminated piezoelectric plates. All of the above Eqs. (2.1)–(2.6) must be satisfied for the material properties of a specific layer. In addition to these equations, the mechanical and electrical boundary conditions on the upper and lower planes must be satisfied:

$$(2.7) \quad \begin{aligned} \sigma_{33}(x_1, h) &= q_0^t \sin px_1, & \sigma_{33}(x_1, 0) &= q_0^b \sin px_1, \\ \sigma_{13}(x_1, h) &= 0, & \sigma_{13}(x_1, 0) &= 0, \\ \sigma_{23}(x_1, h) &= 0, & \sigma_{23}(x_1, 0) &= 0, \\ \varphi(x_1, h) &= \varphi_0^t \sin px_1 \quad \text{or} \quad D_3(x_1, h) = 0, \\ \varphi(x_1, 0) &= \varphi_0^b \sin px_1 \quad \text{or} \quad D_3(x_1, 0) = 0. \end{aligned}$$

The interlaminar continuity conditions on the interfaces between the layers must be also ensured:

$$(2.8) \quad \begin{aligned} \sigma_{3i}^{(k)}(x_1, z_{k+1}) &= \sigma_{3i}^{(k+1)}(x_1, z_{k+1}), & u_i^{(k)}(x_1, z_{k+1}) &= u_i^{(k+1)}(x_1, z_{k+1}), \\ \varphi^{(k)}(x_1, z_{k+1}) &= \varphi^{(k+1)}(x_1, z_{k+1}), & D_3^{(k)}(x_1, z_{k+1}) &= D_3^{(k+1)}(x_1, z_{k+1}), \end{aligned}$$

where q_0^t , q_0^b , φ_0^t and φ_0^b are known constants, $p = n\pi/L$ and n is a positive integer. It is worthy to note that any applied traction load or prescribed electric potential on the surfaces of an FGP plate can be expanded in terms of a Fourier series.

3. Exact solution

A solution in the following form is sought for the displacement components and the electric potential of the k th lamina

$$(3.1) \quad \begin{aligned} u_1^{(k)}(x_1, x_3) &= U^{(k)}(x_3) \cos px_1, & u_2^{(k)}(x_1, x_3) &= V^{(k)}(x_3) \cos px_1, \\ u_3^{(k)}(x_1, x_3) &= W^{(k)}(x_3) \sin px_1, & \varphi^{(k)}(x_1, x_3) &= \Phi^{(k)}(x_3) \sin px_1. \end{aligned}$$

The above assumed solution is reasonable because the applied loads (mechanical and/or electrical) and material properties are independent of x_2 . Moreover, the laminated plate is of infinite extent in the x_2 -direction. Indeed, the laminate is in a generalized plane state of deformation. It can be also observed that Eqs. (3.1) satisfy the boundary conditions (2.5)–(2.6) on the edges $x_1 = 0$ and L . It is worthy to note that no assumption for $U^{(k)}(x_3)$, $V^{(k)}(x_3)$, $W^{(k)}(x_3)$ and $\Phi^{(k)}(x_3)$ is introduced in Eq. (3.1). They are unknown functions that must be determined. Substitution of (3.1) into (2.2)–(2.3) and the result into (2.1) gives the following expressions for the stresses and electric displacements

$$(3.2) \quad \begin{aligned} \sigma_{11}^{(k)} &= \left(-pc_{11}^{(k)}(x_3)U^{(k)}(x_3) + c_{13}^{(k)}(x_3)\frac{dW^{(k)}(x_3)}{dx_3} \right. \\ &\quad \left. - pc_{16}^{(k)}(x_3)V^{(k)}(x_3) + e_{31}^{(k)}(x_3)\frac{d\Phi^{(k)}(x_3)}{dx_3} \right) \sin px_1, \\ \sigma_{22}^{(k)} &= \left(-pc_{12}^{(k)}(x_3)U^{(k)}(x_3) + c_{23}^{(k)}(x_3)\frac{dW^{(k)}(x_3)}{dx_3} \right. \\ &\quad \left. - pc_{26}^{(k)}(x_3)V^{(k)}(x_3) + e_{32}^{(k)}(x_3)\frac{d\Phi^{(k)}(x_3)}{dx_3} \right) \sin px_1, \\ \sigma_{33}^{(k)} &= \left(-pc_{13}^{(k)}(x_3)U^{(k)}(x_3) + c_{33}^{(k)}(x_3)\frac{dW^{(k)}(x_3)}{dx_3} \right. \\ &\quad \left. - pc_{36}^{(k)}(x_3)V^{(k)}(x_3) + e_{33}^{(k)}(x_3)\frac{d\Phi^{(k)}(x_3)}{dx_3} \right) \sin px_1, \\ \sigma_{12}^{(k)} &= \left(-pc_{16}^{(k)}(x_3)U^{(k)}(x_3) + c_{36}^{(k)}(x_3)\frac{dW^{(k)}(x_3)}{dx_3} \right. \\ &\quad \left. - pc_{66}^{(k)}(x_3)V^{(k)}(x_3) + e_{36}^{(k)}(x_3)\frac{d\Phi^{(k)}(x_3)}{dx_3} \right) \sin px_1, \\ \sigma_{23}^{(k)} &= \left(c_{44}^{(k)}(x_3)\frac{dV^{(k)}(x_3)}{dx_3} + c_{45}^{(k)}(x_3)\frac{dU^{(k)}(x_3)}{dx_3} \right. \\ &\quad \left. + pc_{45}^{(k)}(x_3)W^{(k)}(x_3) + pe_{14}^{(k)}(x_3)\frac{d\Phi^{(k)}(x_3)}{dx_3} \right) \cos px_1, \end{aligned}$$

$$\begin{aligned}
\sigma_{13}^{(k)} &= \left(c_{45}^{(k)}(x_3) \frac{dV^{(k)}(x_3)}{dx_3} + c_{55}^{(k)}(x_3) \frac{dU^{(k)}(x_3)}{dx_3} \right. \\
&\quad \left. + p c_{55}^{(k)}(x_3) W^{(k)}(x_3) + p e_{15}^{(k)}(x_3) \frac{d\Phi^{(k)}(x_3)}{dx_3} \right) \cos px_1, \\
D_1^{(k)} &= \left(e_{14}^{(k)}(x_3) \frac{dV^{(k)}(x_3)}{dx_3} + e_{15}^{(k)}(x_3) \frac{dU^{(k)}(x_3)}{dx_3} \right. \\
(3.2) \quad &\quad \left. + p e_{15}^{(k)}(x_3) W^{(k)}(x_3) - p \chi_{11}^{(k)}(x_3) \frac{d\Phi^{(k)}(x_3)}{dx_3} \right) \cos px_1, \\
D_2^{(k)} &= \left(e_{24}^{(k)}(x_3) \frac{dV^{(k)}(x_3)}{dx_3} + e_{25}^{(k)}(x_3) \frac{dU^{(k)}(x_3)}{dx_3} \right. \\
&\quad \left. + p e_{25}^{(k)}(x_3) W^{(k)}(x_3) - p \chi_{12}^{(k)}(x_3) \frac{d\Phi^{(k)}(x_3)}{dx_3} \right) \cos px_1, \\
D_3^{(k)} &= \left(-p e_{31}^{(k)}(x_3) U^{(k)}(x_3) + e_{33}^{(k)}(x_3) \frac{dW^{(k)}(x_3)}{dx_3} \right. \\
&\quad \left. - p e_{36}^{(k)}(x_3) V^{(k)}(x_3) - \chi_{33}^{(k)}(x_3) \frac{d\Phi^{(k)}(x_3)}{dx_3} \right) \sin px_1.
\end{aligned}$$

Substitution of (3.2) into the governing equations (2.4), and writing the resulting system of second-order differential equations as a set of first-order differential equations, the following state space matrix equation can be obtained

$$(3.3) \quad \mathbf{K}^{(k)} \mathbf{X}_{,3}^{(k)} + \mathbf{B}^{(k)} \mathbf{X}^{(k)} = 0$$

or

$$(3.4) \quad \mathbf{X}_{,3}^{(k)} = \mathbf{A}^{(k)} \mathbf{X}^{(k)},$$

where

$$(3.5) \quad \mathbf{A}^{(k)} = -(\mathbf{K}^{(k)})^{-1} \mathbf{B}^{(k)},$$

$$\mathbf{K}^{(k)} = \begin{bmatrix} 1 & 0 & 0 & 0 & 0 & 0 & 0 & 0 \\ 0 & 1 & 0 & 0 & 0 & 0 & 0 & 0 \\ 0 & 0 & 1 & 0 & 0 & 0 & 0 & 0 \\ 0 & 0 & 0 & 1 & 0 & 0 & 0 & 0 \\ 0 & 0 & 0 & 0 & c_{55}(x_3) & c_{45}(x_3) & 0 & 0 \\ 0 & 0 & 0 & 0 & c_{45}(x_3) & c_{44}(x_3) & 0 & 0 \\ 0 & 0 & 0 & 0 & 0 & 0 & c_{33}(x_3) & e_{33}(x_3) \\ 0 & 0 & 0 & 0 & 0 & 0 & e_{33}(x_3) & -\chi_{33}(x_3) \end{bmatrix},$$

$$\mathbf{B}^{(k)} = \begin{bmatrix} 0 & 0 & 0 & 0 & -1 \\ 0 & 0 & 0 & 0 & 0 \\ 0 & 0 & 0 & 0 & 0 \\ 0 & 0 & 0 & 0 & 0 \\ -p^2 c_{11}(x_3) & -p^2 c_{16}(x_3) & p \frac{dc_{55}(x_3)}{dx_3} & p \frac{de_{15}(x_3)}{dx_3} & \frac{dc_{55}(x_3)}{dx_3} \\ -p^2 c_{16}(x_3) & -p^2 c_{66}(x_3) & p \frac{dc_{45}(x_3)}{dx_3} & p \frac{de_{14}(x_3)}{dx_3} & \frac{dc_{45}(x_3)}{dx_3} \\ -p \frac{dc_{13}(x_3)}{dx_3} & -p \frac{dc_{36}(x_3)}{dx_3} & -p^2 c_{55}(x_3) & -p^2 e_{15}(x_3) & -p(c_{55}(x_3) + c_{13}(x_3)) \\ -p \frac{de_{31}(x_3)}{dx_3} & -p \frac{de_{36}(x_3)}{dx_3} & -p^2 e_{15}(x_3) & p^2 \chi_{11}(x_3) & -p(e_{15}(x_3) + e_{31}(x_3)) \\ & 0 & 0 & 0 & \\ & -1 & 0 & 0 & \\ & 0 & -1 & 0 & \\ & 0 & 0 & -1 & \\ & \frac{dc_{45}(x_3)}{dx_3} & p(c_{13}(x_3) + c_{55}(x_3)) & p(e_{31}(x_3) + e_{15}(x_3)) & \\ & \frac{dc_{44}(x_3)}{dx_3} & p(c_{36}(x_3) + c_{45}(x_3)) & p(e_{36}(x_3) + e_{14}(x_3)) & \\ -p(c_{45}(x_3) + c_{36}(x_3)) & & \frac{dc_{33}(x_3)}{dx_3} & \frac{de_{33}(x_3)}{dx_3} & \\ -p(e_{14}(x_3) + e_{36}(x_3)) & & \frac{de_{33}(x_3)}{dx_3} & -\frac{d\chi_{33}(x_3)}{dx_3} & \end{bmatrix},$$

$$\mathbf{X}^{(k)} =$$

$$\left[U^{(k)}(x_3) \ V^{(k)}(x_3) \ W^{(k)}(x_3) \ \Phi^{(k)}(x_3) \ \frac{dU^{(k)}(x_3)}{dx_3} \ \frac{dV^{(k)}(x_3)}{dx_3} \ \frac{dW^{(k)}(x_3)}{dx_3} \ \frac{d\Phi^{(k)}(x_3)}{dx_3} \right]^T.$$

For the homogeneous piezoelectric layers, the matrix $\mathbf{A}^{(k)}$ in basic Eq. (3.4) reduces to a homogenous constant matrix. In this case, the solution of Eq. (3.4) can be written as [36–37]:

$$(3.6) \quad \mathbf{X}^{(k)} = \exp[\mathbf{A}^{(k)} x_3] \delta^{(k)},$$

where $\delta^{(k)}$ is an 8×1 vector of unknown constants. In the particular case where the piezoelectric layers have an exponent-law dependence on the thickness-coordinate, the matrices $\mathbf{K}^{(k)}$ and $\mathbf{B}^{(k)}$ have the factorized inhomogeneity $\mathbf{K}^{(k)} \propto \exp(ax_3)$, $\mathbf{B}^{(k)} \propto \exp(ax_3)$ (a is a constant characterizing the degree of the material gradient along x_3). Thus, in this particular case, the matrix $\mathbf{A}^{(k)}$ in Eq. (3.4) becomes a homogenous constant matrix, and Eq. (3.6) is still a valid solution for the basic Eq. (3.4). This fact specifies why the previous authors in [32] and other similar works have limited themselves to the consideration of plates with the exponential variation of the mechanical and electrical properties along the thickness direction. For the FGP layers with arbitrary compositional gradient, it is obvious that the components of matrix $\mathbf{A}^{(k)}$ in Eq. (3.4) are not

constants. It is evident that they are now functions of the coordinate x_3 . Thus, the typical solution $\mathbf{X}^{(k)} = \exp[\mathbf{A}^{(k)}x_3]\boldsymbol{\delta}^{(k)}$ is no longer valid for Eq. (3.4). In mathematics and mechanics of inhomogeneous media, the solution to Eq. (3.4) can be written as [36–43]:

$$(3.7) \quad \mathbf{X}^{(k)} = \mathbf{W}^{(k)}(x_3)\boldsymbol{\delta}^{(k)},$$

where $\mathbf{W}^{(k)}(x_3) = \text{Ord} \exp[\int_0^{x_3} \mathbf{A}^{(k)}(x)dx]$ is called the propagator matrix, which can be expressed as the following Peano expansion [36–37]:

$$(3.8) \quad \mathbf{W}^{(k)}(x_3) = \mathbf{I} + \int_0^{x_3} \mathbf{A}^{(k)}(x)dx + \int_0^{x_3} \mathbf{A}^{(k)}(x) \int_0^x \mathbf{A}^{(k)}(y_1)dy_1dx \\ + \int_0^{x_3} \mathbf{A}^{(k)}(x) \int_0^x \mathbf{A}^{(k)}(y_1) \int_0^{y_1} \mathbf{A}^{(k)}(y_2)dy_2dy_1dx + \dots$$

Thus, the solutions for the displacement components u_i and the electric potential φ are expressed in terms of eight unknown constants for each of the N layers. This yields $8N$ total unknowns for the complete graded piezoelectric laminated plate. These constants are determined by satisfying the boundary and interface continuity conditions at the upper and lower surfaces of each layer. There are four boundary conditions at the top of layer N_l and the bottom of layer 1, with a total of eight boundary conditions (Eq. (2.7)). At each interface the continuity conditions as expressed in Eq. (2.8) must be ensured, leading to $8(N_l - 1)$ equations. Thus, the total number of equations and unknowns is $8N_l$ which can be easily solved. Once the constants are determined, the mechanical displacements, stresses, electric potential and electric displacement can be evaluated at any location within the FGP laminate.

4. Numerical results and discussion

In this section, some numerical examples are considered to ascertain the accuracy of the proposed exact state-space solution. To this end, results of the present formulation are compared with available previously published results. Although the first two examples of the present section are mainly devoted to the verification purposes, the third example included in this section contains new results.

4.1. Example 1

A single layer FGP plate with the length $L = 1$ m and length-to-thickness ratio $S = 1$ is considered in this example. The plate is made of a PZT-4 based exponentially graded piezoelectric with the following material properties:

$$c_{kl} = c_{kl}^0 f(x_3), \quad e_{ik} = e_{ik}^0 f(x_3), \quad \chi_{ij} = \chi_{ij}^0 f(x_3),$$

where

$$f(x_3) = e^{ax_3}, \quad 0 < x_3 < 1$$

and a is a constant characterizing the degree of the material gradient along x_3 , c_{kl}^0 , e_{ik}^0 and χ_{ij}^0 are the values of material properties at the plane $x_3 = 0$. The mechanical and electrical properties of PZT-4 are cited in Table 1. The plate is simply supported along two edges. The exact electro-mechanical solution for this graded piezoelectric plate has been previously obtained by LU *et al.* [33] based on the Stroh-like formalism. Accuracy of the results of the present state-space formulation is evaluated by comparing the obtained results with those obtained in [33]. The low value of the length-to-thickness ratio employed in [33] help to assess the effect of gradient index a on the distribution of stresses, electric displacements, displacements and electric potential with more clarity.

Table 1. Mechanical and electrical properties of some piezoelectric materials.

	PZT-4	PZT-5H
c_{11}^0 (GPa)	139	127.20
c_{12}^0 (GPa)	77.8	80.21
c_{22}^0 (GPa)	139	127.20
c_{13}^0 (GPa)	74.3	84.67
c_{23}^0 (GPa)	74.3	84.67
c_{33}^0 (GPa)	115	117.44
c_{44}^0 (GPa)	25.6	22.99
c_{55}^0 (GPa)	25.6	22.99
c_{66}^0 (GPa)	30.6	23.47
e_{15}^0 (Cm ⁻²)	12.7	17.03
e_{24}^0 (Cm ⁻²)	12.7	17.03
e_{31}^0 (Cm ⁻²)	-5.2	-6.62
e_{32}^0 (Cm ⁻²)	-5.2	-6.62
e_{33}^0 (Cm ⁻²)	15.1	23.24
χ_{11}^0 (10 ⁻⁸ Fm ⁻¹)	1.306	2.771
χ_{22}^0 (10 ⁻⁸ Fm ⁻¹)	1.306	2.771
χ_{33}^0 (10 ⁻⁸ Fm ⁻¹)	1.151	3.010
ρ (kg/m ³)	7500	7500

Actuator case. The FGP plate is first subjected to a top sine potential along the length of the laminate with peak amplitude of 1 ($\varphi(x_1, h) = \sin \pi x_1/L$). The bottom plane of the plate is electrically grounded. The top and bottom planes of the plate are traction-free. The variation of displacements u_1 and u_3 , stresses σ_{11} , σ_{22} , σ_{33} and σ_{13} , transverse electric displacement D_3 , and electric potential

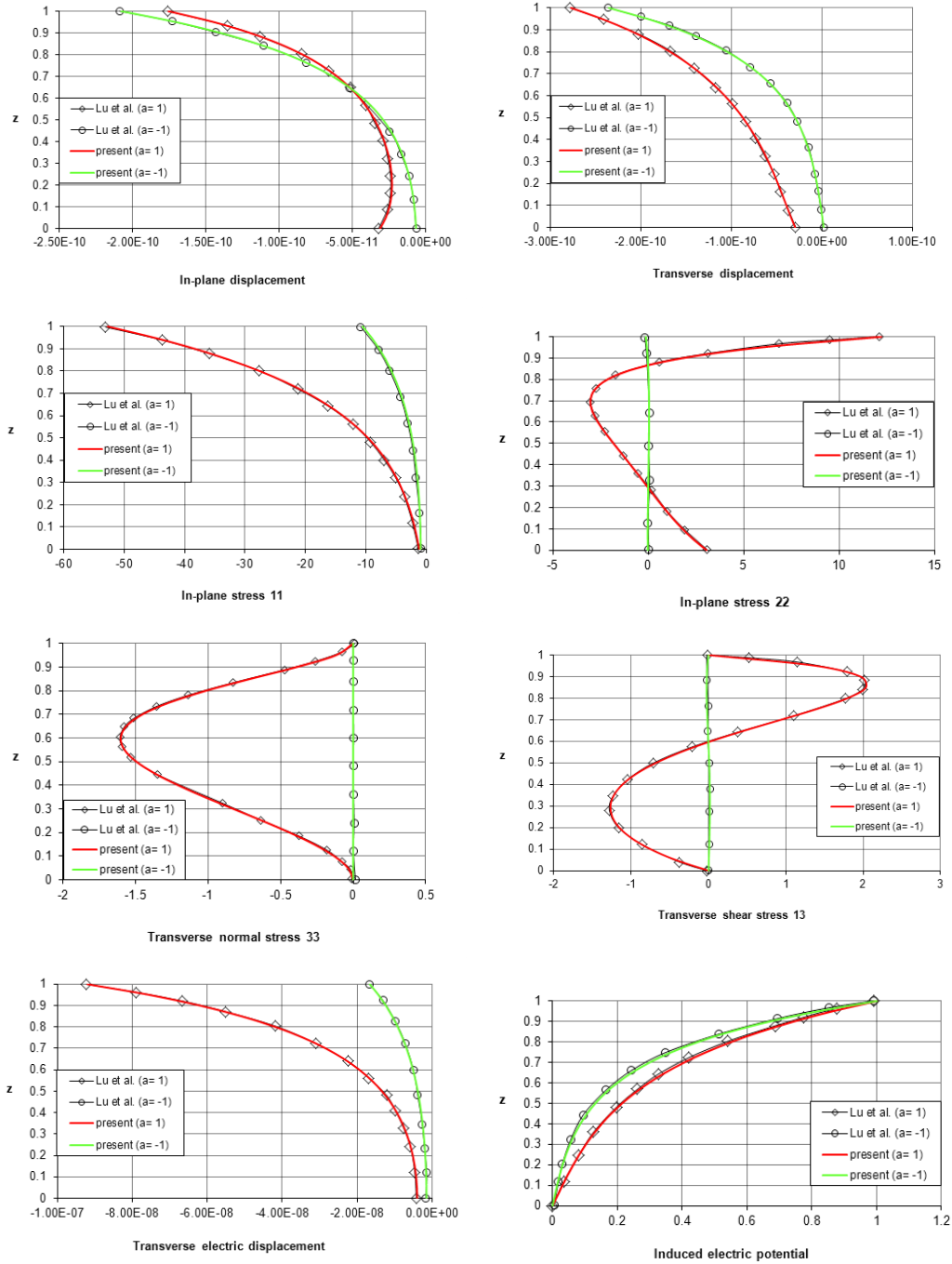


FIG. 2. Through-the-thickness variations of u_1 , u_3 , σ_{11} , σ_{22} , σ_{33} , σ_{13} , D_3 and φ in the single layer functionally graded piezoelectric plate under the sinusoidal electric potential.

φ are shown in Fig. 2 as a function of the plate thickness coordinate x_3 . In these figures, the material property gradient index a is taken for two values: $-1, 1$.

The numerical results for the aforementioned quantities are also presented in Table 2. Since the 3D solutions by LU *et al.* [33] were unfortunately only given in graphic forms, only a few significant digits are considered in this table. All the numerical results are calculated across $0 < x_3 < 1$ on the section $x_1 = 0.25L$. It is seen that the excellent agreement exists between the present results with those obtained from the Stroh-like formalism of LU *et al.* [33]. In comparison to the Stroh-like formalism of LU *et al.* [33] which is restricted to the analysis of FGP plate with the exponential variation of the mechanical and electrical properties along the thickness direction, the present state-space solution considers piezoelectric materials with arbitrary compositional gradient. From Fig. 2, we discover that the gradient index a will influence the distribution of stresses, electric displacements, displacements and electric potential in different degree. The depicted graphs of Fig. 2 also reveal that under a similar electric force, the transverse deflection of the plate made of hard gradient materials ($a = +1$) is higher than the plate made of soft gradient materials ($a = -1$). The maximal absolute values of stress components and transverse electric displacement of the graded plate made of hard piezoelectric materials are also higher than soft one. For $a = 1$, the maximal absolute value of D_3 is 5.54 times larger than that of $a = -1$. The maximal absolute value of σ_{11} is also 5.01 times larger than that of $a = -1$. Such behaviors can be interpreted using the coupled electromechanical properties of piezoelectric materials. Due to its higher electromechanical stiffness, the induced mechanical deformations of the hard

Table 2. Results for the actuated single layer functionally graded piezoelectric plate under sinusoidal electric potential.

	a	Present	LU <i>et al.</i> [33]
$u_1(0.25L, h) \times 10^{10}$	1	-1.758	-1.762
	-1	-2.080	-2.089
$u_3(0.25L, h) \times 10^{10}$	1	-2.769	-2.777
	-1	-2.353	-2.356
$\sigma_{11}(0.25L, h)$	1	-52.751	-53.695
	-1	-10.531	-10.633
$\sigma_{33}(0.25L, 0.6h)$	1	-1.603	-1.607
	-1	0.000	0.000
$\sigma_{13}(0.25L, 0.3h)$	1	-1.269	-1.258
	-1	0.019	0.018
$D_3(0.25L, h) \times 10^8$	1	-9.200	-9.204
	-1	-1.661	-1.669

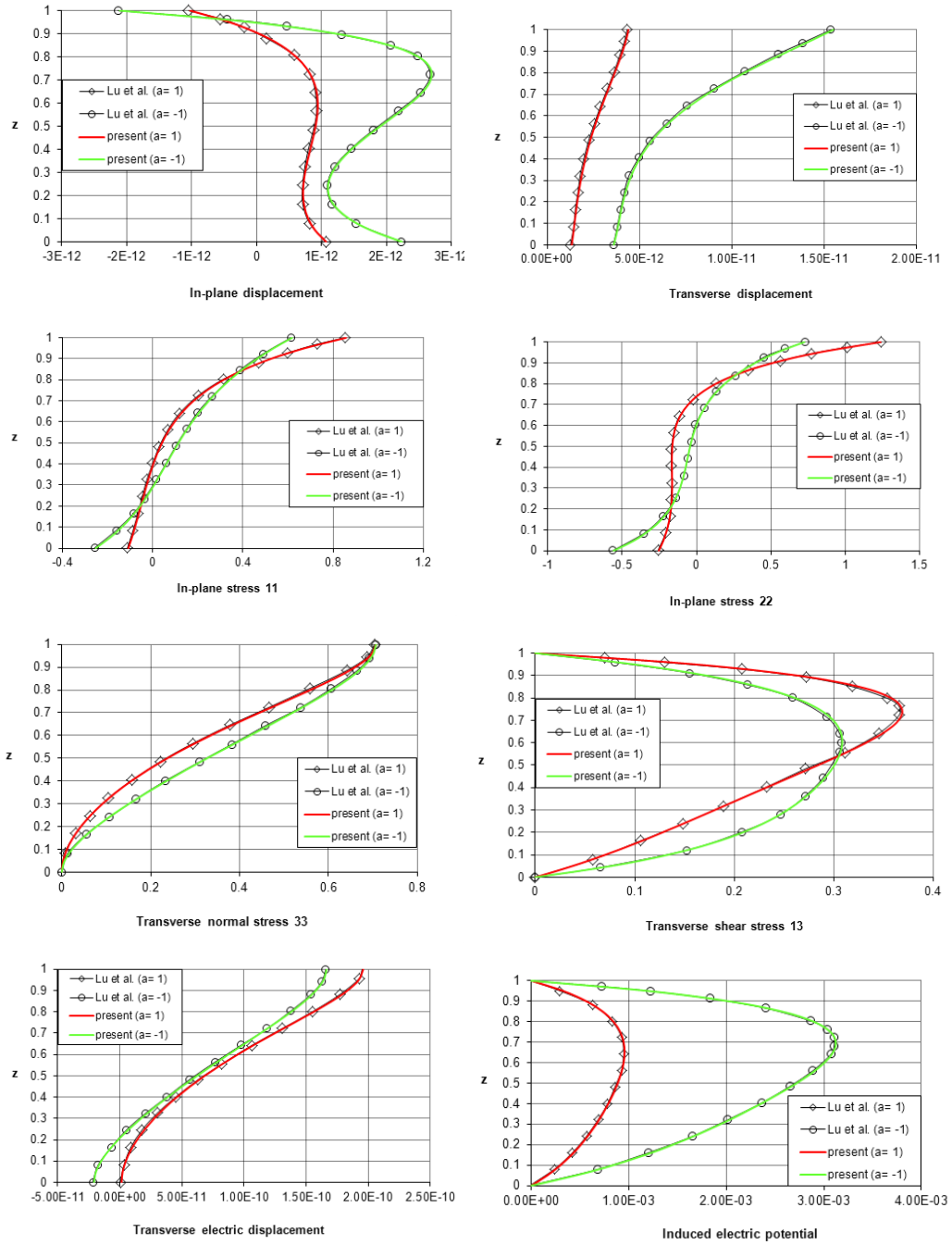


FIG. 3. Through-the-thickness distributions of u_1 , u_3 , σ_{11} , σ_{22} , σ_{33} , σ_{13} , D_3 and φ in the single layer graded piezoelectric plate under the sinusoidal mechanical force – CC electric boundary conditions.

FGP plate will be more than the soft one. Consequently, the maximal values of stress components in the hard FGP plate will be more than the soft one. Although it seems that the hard gradient materials are more effective actuators than soft ones, the possible failure material in them are also higher than in soft ones.

Sensor case. In the next case, the mechanical force $\sigma_{33}(x_1, h) = \sin \pi x_1/L$ is applied to the top of the FGP plate. Through-the-thickness distributions of u_1 , u_3 , σ_{11} , σ_{22} , σ_{33} , σ_{13} , D_3 and φ with closed circuit (CC) electric boundary conditions are shown in Fig. 3 at the chosen point $x_1 = 0.25L$. For further comparison, the results are also summarized in Table 3. Similar to the actuator case, the numerical results obtained from the present state-space formulation exhibit excellent agreements with the results obtained by the Stroh-like formalism of LU *et al.* [33]. These obtained numerical results justify the accuracy of the proposed 3D exact state-space formulation for the electro-mechanical analysis of FGP plates. Moreover, it can be observed from Fig. 3 that the mechanical deformations of the plate made of soft gradient materials are higher than the plate made of hard gradient materials while its maximal absolute values of stress components are lower. For $a = 1$, the maximal deflection of plate is 6.53 times larger than that of $a = -1$, while the corresponding transverse shear stress is 0.84 times lower than that of $a = -1$. Due to the fact that the electromechanical stiffness of the graded plate made of hard piezoelectric materials are higher than soft one, such behaviors are expected. Figure 3 shows also that the induced electric potential in the soft FGP plate is higher than hard one (3.27 times). Under mechanical loadings, the soft piezoelectric plate undergoes more mechanical deformations and consequently converts more mechanical energy into the electrical energy.

Table 3. Results for the sensory single layer functionally graded piezoelectric plate under sinusoidal mechanical force.

	a	Present	LU <i>et al.</i> [33]
$u_1(0.25L, h) \times 10^{12}$	1	-1.024	-1.046
	-1	-2.107	-2.135
$u_3(0.25L, h) \times 10^{11}$	1	0.440	0.433
	-1	1.550	1.537
$\sigma_{11}(0.25L, h)$	1	0.858	0.852
	-1	0.618	0.613
$\sigma_{13}(0.25L, 0.6h)$	1	0.332	0.331
	-1	0.308	0.308
$\varphi(0.25L, 0.7h) \times 10^3$	1	0.945	0.951
	-1	3.121	3.127

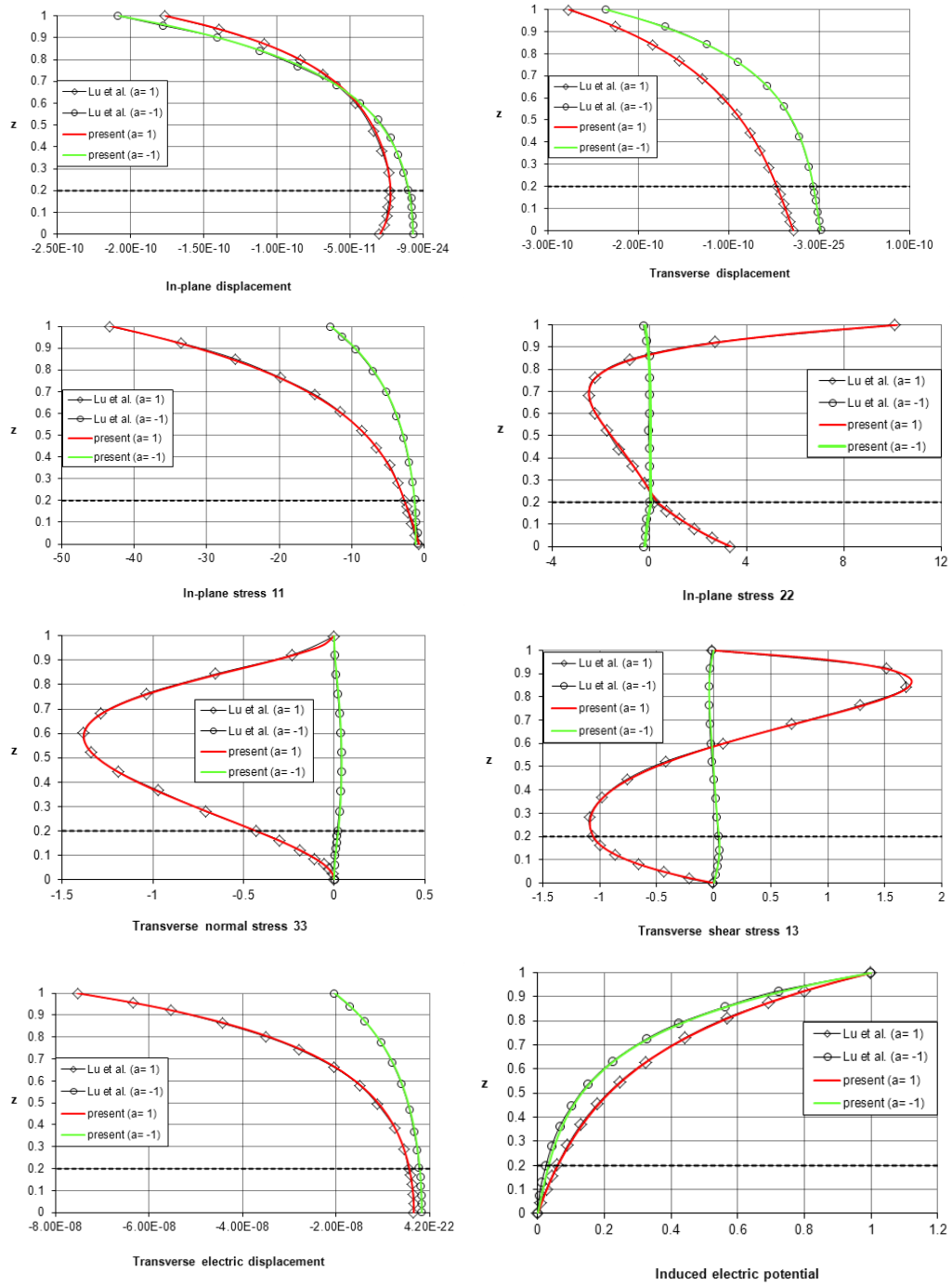


FIG. 4. Through-the-thickness variations of u_1 , u_3 , σ_{11} , σ_{22} , σ_{33} , σ_{13} , D_3 and φ in the two-layer functionally graded piezoelectric plate under the sinusoidal electric potential.

4.2. Example 2

In this example, a two-layered FGP plate with the length $L = 1$ m and length-to-thickness ratio $S = 1$ is considered. The lower layer is made of a homogenous PZT-4 piezoelectric material. The upper layer is a PZT-4 based exponentially graded piezoelectric layer with the following material properties:

$$c_{kl} = c_{kl}^0 f(x_3), \quad e_{ik} = e_{ik}^0 f(x_3), \quad \chi_{ij} = \chi_{ij}^0 f(x_3),$$

where

$$f(x_3) = e^{a(x_3-0.2)}, \quad 0.2 < x_3 < 1.$$

The ratio of the upper graded layer to the lower homogenous layer has been taken as 4. It is pointed out that c_{kl}^0 , e_{ik}^0 and χ_{ij}^0 in the present example are the values of material properties at the bottom of top layer. Similar to the previous example, all the numerical results are calculated across $0 < x_3 < 1$ on the section $x_1 = 0.25L$. Concerning the material property gradient index a , two values: -1 , 1 are chosen. The obtained numerical results have been compared with the results obtained from the Stroh-like formalism of LU *et al.* [33].

Actuator case. A sine potential with peak amplitude of 1 is applied to the top of the two layered FGP plate. The top and bottom planes of the plate are traction-free. The bottom plane of the graded plate is assumed to be electrically grounded. The numerical results for displacements u_1 and u_3 , stresses σ_{11} , σ_{22} , σ_{33} and σ_{13} , transverse electric displacement D_3 , and electric potential φ are presented in Fig. 4 and summarized in Table 4. It is seen again that

Table 4. Results for the actuated two-layer functionally graded piezoelectric plate under sinusoidal electric potential.

	a	Present	LU <i>et al.</i> [33]
$u_1(0.25L, h) \times 10^{10}$	1	-1.762	-1.766
	-1	-2.077	-2.081
$u_3(0.25L, h) \times 10^{10}$	1	-2.763	-2.767
	-1	-2.357	-2.359
$\sigma_{11}(0.25L, h)$	1	-43.119	-43.168
	-1	-12.870	-12.898
$\sigma_{33}(0.25L, 0.6h)$	1	-1.379	-1.381
	-1	0.038	0.039
$\sigma_{13}(0.25L, 0.2h)$	1	-1.057	-1.063
	-1	0.046	0.047
$D_3(0.25L, h) \times 10^8$	1	-7.534	-7.524
	-1	-2.028	-2.025

the present state-space results are in excellent agreements with the LU *et al.*'s solution [33]. Considering various values for aspect ratio, the normalized transverse displacement (\tilde{u}_3) obtained at the middle of the simply supported FGP plate is also shown in Fig. 5 for three values of the material property gradient index $a = -1, 0, 1$. Note that when $a=0$, the plate is a homogenous one made of material PZT-4. It is seen that the increasing of \tilde{u}_3 is significant when $L/h < 10$, but when $L/h > 10$ all curves tend to be horizontal indicating that \tilde{u}_3 becomes almost invariant. The obtained numerical results of this chart can be used as benchmarks to assess the accuracy of different 2D FGP plate theories.

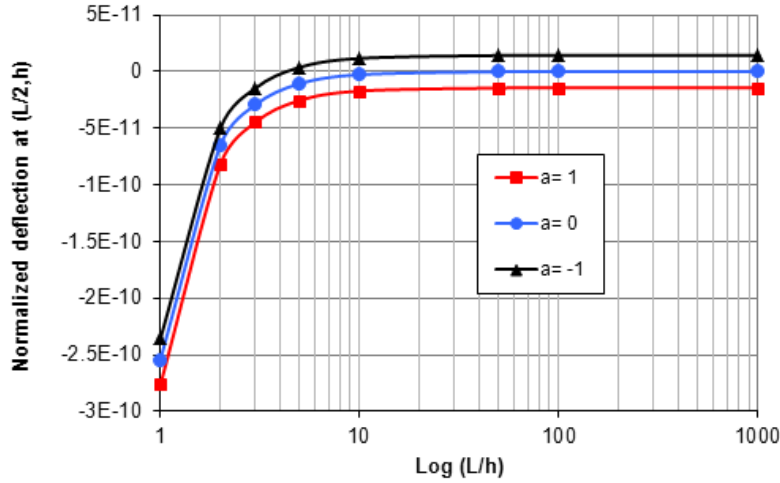


FIG. 5. Variation of the normalized transverse displacement $\tilde{u}_3 = u_3(L/2, h)/S^2$ with respect to aspect ratio – the two-layer functionally graded piezoelectric plate under the sinusoidal electric potential.

Sensor case. The mechanical force $\sigma_{33}(x_1, h) = \sin \pi x_1/L$ is applied to the top plane of the FGP plate. The variations of mechanical and electrical responses with open circuit (OC) electric boundary conditions are depicted in Fig. 6 as a function of the plate thickness coordinate x_3 . The corresponding numerical results are also presented in Table 5 for further comparison. The excellent agreement between the present results with those obtained from Stroh-like formalism can be observed. It is seen from these figures that the nonlinear distribution of u_1 , u_3 and φ along the thickness direction increases with decreasing of the material gradient index. Therefore, the available two-dimensional laminated plate theories do not seem to be able to predict accurately the electromechanical response of FGP plates made of soft materials. This means that more refined plate theories

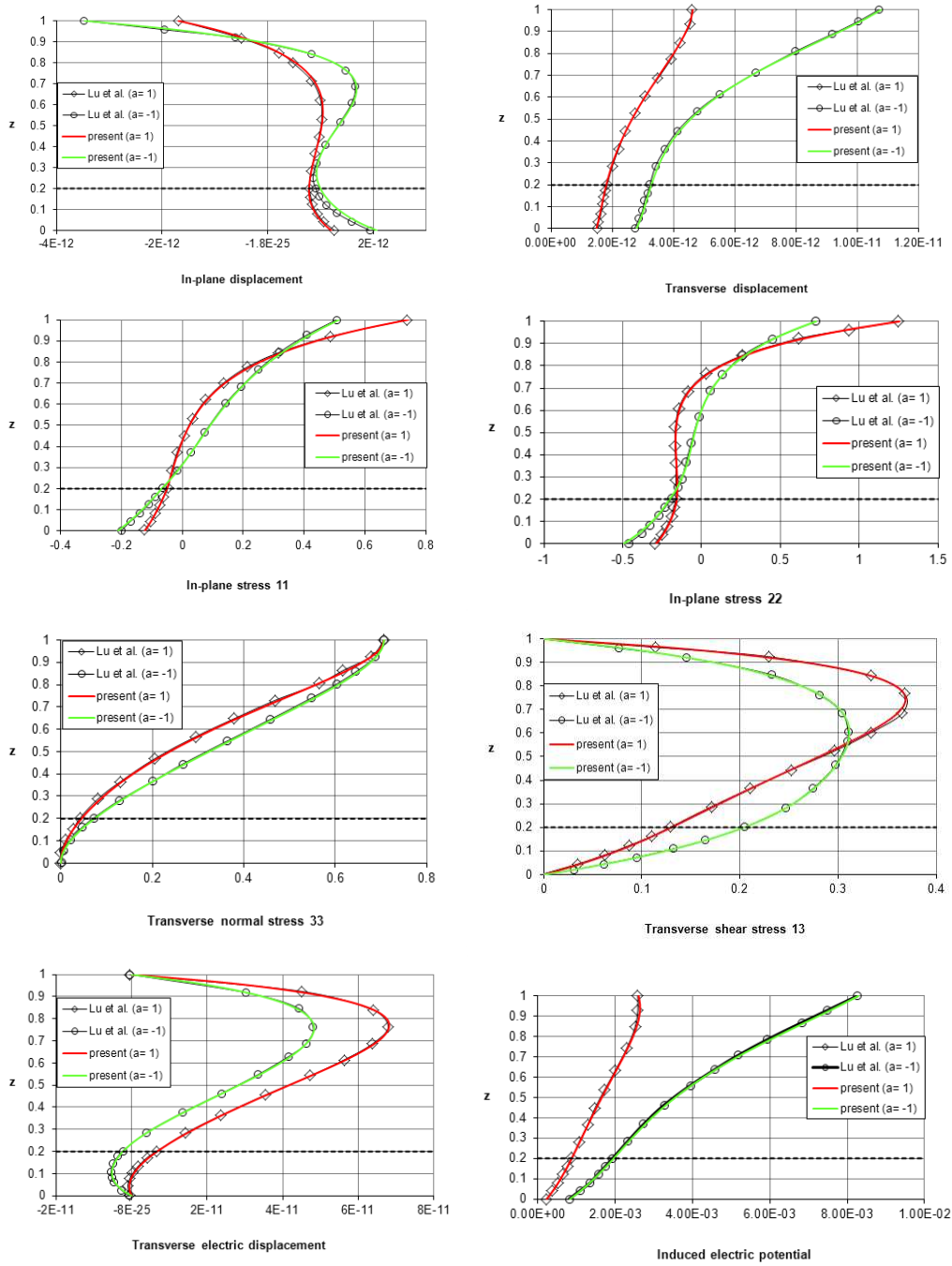


FIG. 6. Through-the-thickness distributions of u_1 , u_2 , σ_{11} , σ_{22} , σ_{33} , σ_{13} , D_3 and φ in the two-layer graded piezoelectric plate under the sinusoidal mechanical force – OC electric boundary conditions.

Table 5. Results for the sensory two-layer functionally graded piezoelectric plate under sinusoidal mechanical force.

	a	Present	LU <i>et al.</i> [33]
$u_1(0.25L, h) \times 10^{12}$	1	-1.694	-1.684
	-1	-3.466	-3.454
$u_3(0.25L, h) \times 10^{11}$	1	0.462	0.458
	-1	1.078	1.071
$\sigma_{11}(0.25L, h)$	1	0.742	0.737
	-1	0.514	0.507
$\sigma_{13}(0.25L, 0.6h)$	1	0.330	0.334
	-1	0.11	0.311
$\varphi(0.25L, 0.7h) \times 10^3$	1	2.604	2.585
	-1	8.285	8.257

are needed for the analysis of functionally graded laminated piezoelectric plates, particularly those made of soft materials.

Figure 7 shows the normalized transverse displacement obtained at the middle of the simply supported FGP plate with respect to various aspect ratios. Similar to the actuator case, the decreasing of the normalized transverse displacement (\bar{u}_3) is considerable when $L/h < 10$. For $L/h > 10$, the change of \bar{u}_3 with respect to the aspect ratio is poor. For assessing the accuracy of different FGP laminated plate theories and/or validating finite element codes, these numerical results will be useful.

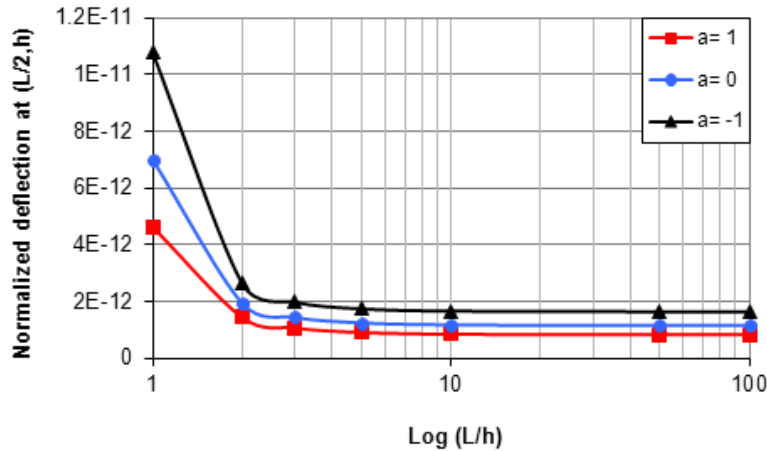


FIG. 7. Variation of the normalized transverse displacement $\bar{u}_3 = u_3(L/2, h)/S^4$ with respect to aspect ratio – the two-layer functionally graded piezoelectric plate under the sinusoidal mechanical force – OC electric boundary conditions.

4.3. Example 3

As the last example, a single layer FGP plate with a total thickness $h = 1$ mm and length $L = 5$ mm is considered. The material properties of this plate vary according to the following power-law distribution:

$$\psi = (1 - f(x_3))\psi^B + f(x_3)\psi^T,$$

where $f(x_3) = \left(\frac{2x_3+h}{2h}\right)^a$ and ψ is an arbitrary material properties of the FGP material. ψ^B and ψ^T represent the values of ψ on the top and bottom of the graded plate respectively. The symbol a is the material gradient index. In the considered plate, the material properties vary from 100% PZT-4 at the top surface to 100% PZT-5H at the bottom surface. The elastic, piezoelectric and dielectric constants for these two piezoelectric materials can be found in Table 1. It is worthy to note that by employing the Stroh-like formalism of LU *et al.* [33], one cannot find the exact 3D solution for the present example. It is due to this fact that the mathematical formulations derived in [33] are valid only for FGP plates whose mechanical and electrical properties along the thickness direction vary according to the exponent-low distribution. However, the material properties of the considered FGP plate of the present example vary according to a power-law distribution. To the knowledge of the authors, there is no exact solution for the analysis of these types of FGP plates in the literature. As stated before, the available exact solutions reported for the analysis of FGP plates either assume that the graded plate consists of a number of homogenous layers or have limited themselves to a consideration of only exponentially graded materials.

Actuator case. The sinusoidal electric potential $\varphi(x_1, h) = \varphi_0 \sin \pi x_1 / L$ is applied to the top of the FGP plate. Through-the-thickness distributions of u_1 , u_3 , σ_{11} , σ_{33} , σ_{13} , D_3 and φ are shown in Fig. 8. The results are also summarized in Table 6 for further comparison. Note that the mechanical and electrical entities are normalized as the below:

Table 6. Results for the actuated FGP plate with material properties varying in a power-law distribution under sinusoidal electric potential.

	a		
	0	1	10
$u_1(0, h) \times 10^{10}$	-3.034	-4.427	-5.749
$u_3(0.5L, h) \times 10^{10}$	-2.623	-1.733	-3.490
$\sigma_{11}(0.5L, h)$	192.940	-1840.900	-5159.270
$\sigma_{33}(0.5L, 0.5h)$	-2.489	17.020	12.032
$\sigma_{13}(0, 0.2h)$	-12.060	74.675	44.831
$D_3(0.5L, h) \times 10^5$	-1.833	-2.891	-4.286

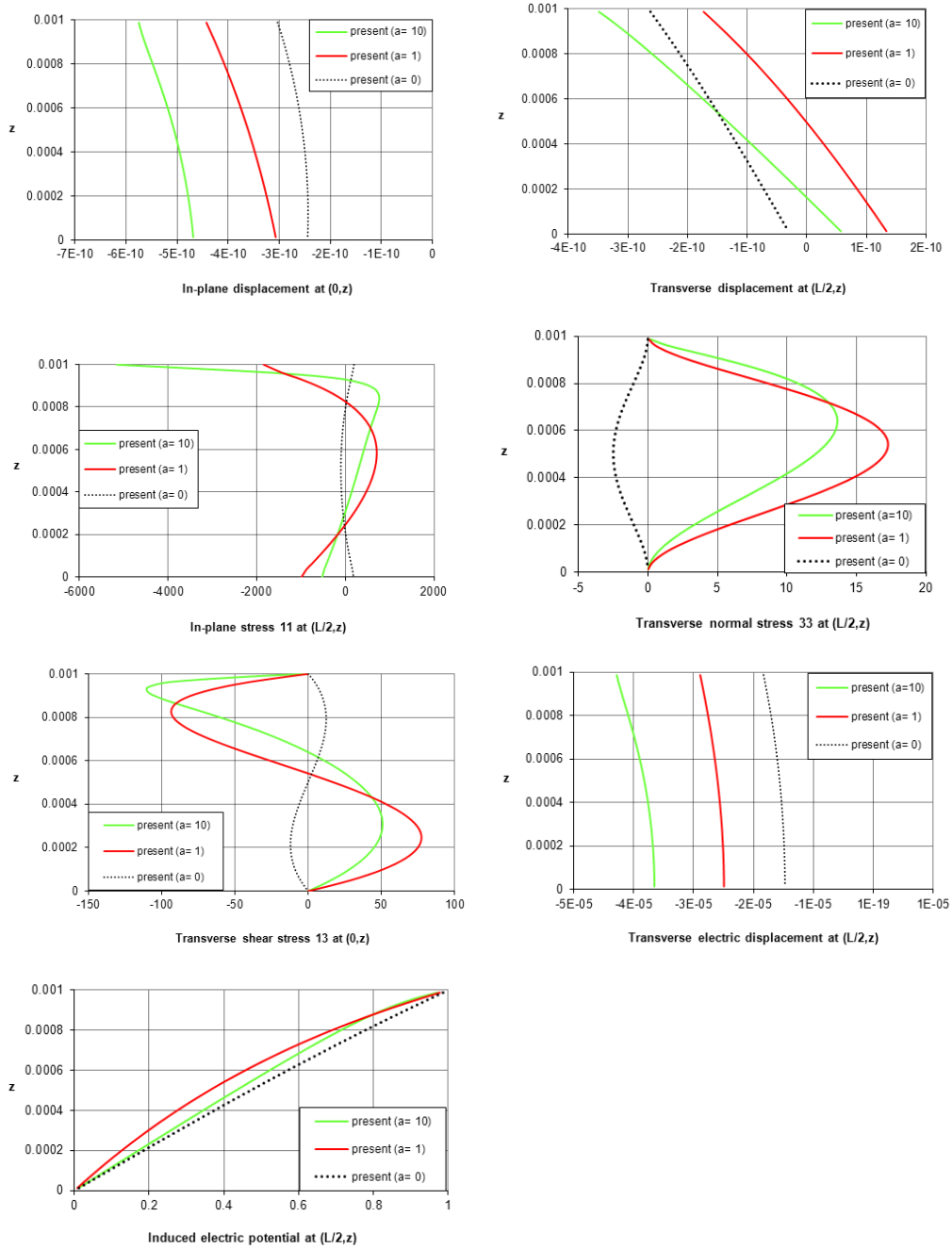


FIG. 8. Through-the-thickness distributions of u_1 , u_2 , σ_{11} , σ_{33} , σ_{13} , D_3 and φ in the piezoelectric plate with material properties varying in a power law under the sinusoidal electric potential.

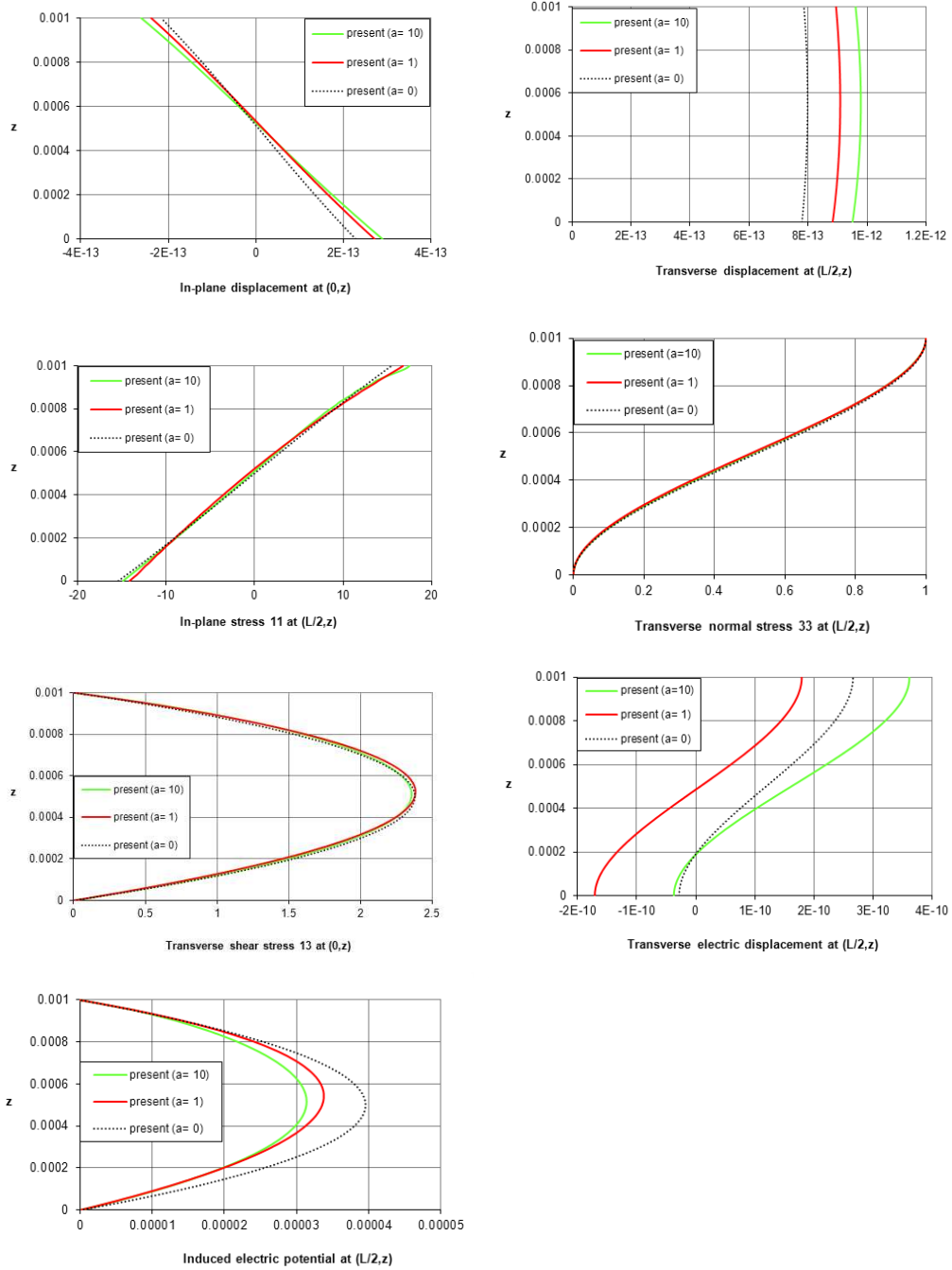


FIG. 9. Through-the-thickness distributions of u_1 , u_2 , σ_{11} , σ_{33} , σ_{13} , D_3 and φ in the piezoelectric plate with material properties varying in a power law under the sinusoidal mechanical force.

$$\bar{\sigma}_{ij} = \sigma_{ij}/\varphi_0, \quad \bar{u}_i = u_i/\varphi_0, \quad \bar{D}_i = D_i/\varphi_0, \quad \bar{\varphi} = \varphi/\varphi_0$$

It is seen that when the material properties are designated at the upper and lower surfaces, the distribution of mechanical and electrical entities are affected by the value of the gradient index a . The a influences the in-plane stress greatly. With the increase of the value a , the in-plane stress at the top of the graded plate increases. In case of $a = 10$, the maximal absolute value of the in-plane stress is as 2.80 times large as that of $a = 1$, and as 9.54 times larger than that of $a = 0$.

Table 7. Results for the sensory FGP plate with material properties varying in a power-law distribution under sinusoidal mechanical force.

	a		
	0	1	10
$u_1(0, h) \times 10^{13}$	-2.169	-2.395	-2.624
$u_3(0.5L, h) \times 10^{13}$	7.862	8.948	9.612
$\sigma_{11}(0.5L, h)$	15.458	16.765	17.511
$\sigma_{13}(0, 0.5h)$	2.378	2.377	2.354
$\varphi(0.5L, 0.5h) \times 10^5$	3.955	3.353	3.135

Sensor case. In this case, the FGP plate is subjected to the action of the sinusoidal mechanical force $\sigma_{33}(x_1, h) = p_0 \sin \pi x_1/L$. The numerical results for displacements u_1 and u_3 , stresses σ_{11} , σ_{33} and σ_{13} , transverse electric displacement D_3 , and electric potential φ are presented in Table 7 and depicted in Fig. 9. The stress and displacement components, the induced electric potential and the electric displacement vector components are normalized as below:

$$\bar{\sigma}_{ij} = \sigma_{ij}/p_0, \quad \bar{\varphi} = \varphi/p_0, \quad \bar{D}_i = D_i/p_0, \quad \bar{\varphi} = \varphi/p_0.$$

From Fig. 9, it can be observed that the gradient index a will influence the distribution of stresses, transverse electric displacement, displacements and electric potential in different degrees. The value of a has little influence on the distribution of stress and displacement components; however, it influences the distribution of the induced electric potential and transverse electric displacement effectively. For $a = 0$, the maximal absolute value of φ is 26% larger than that of $a = 10$.

5. Conclusion

Cylindrical bending of FGP laminated plates is investigated based on the three-dimensional theory of piezoelectricity in the state space setting. For the first time, the exact solution introduced in the present paper is valid for FGP

laminated plates with arbitrary compositional gradient along the thickness direction. However, the proposed state-space solution is very simple, concise and convenient in operation. The present solution is also in excellent agreements with the other exact solutions available in the literature. The obtained numerical results of the present study give a comprehensive insight about the static electro-mechanical behavior of the FGP plates. Moreover, the presented numerical results can play as a benchmark result for validating different FGP plate theories.

Acknowledgements

Author would like to acknowledge the technical discussion and suggestions of Professor M. Shariyat, Department of Mechanical Engineering, K.N. Toosi University of Technology, Tehran, Iran.

References

1. H.S. TZOU, M. GADRE, *Theoretical analysis of a multi-layered thin shell coupled with piezoelectric shell actuators for distributed vibration controls*, J. Sound Vib., **132**, 433–450, 1989.
2. H.S. TZOU, C.I. TSENG, *Distributed piezoelectric sensor/actuator design for dynamic measurement /control of distributed parameter systems: a piezoelectric finite element approach*, J. Sound Vib., **138**, 1, 17–34, 1990.
3. D.A. SARAVANOS, P.R. HEYLIGER, *Coupled layer-wise analysis of composite beams with embedded piezoelectric sensors and actuators*, J. Intell. Mater. Syst. Struct., **6**, 350–363, 1995.
4. P.R. Heyliger, D.A. Saravanos, *Coupled discrete-layer finite elements for laminated piezoelectric plates*, Commun. Numer. Methods Eng., **10**, 12, 971–981, 1994.
5. P.R. HEYLIGER, S.B. BROOKS, *Exact free vibration of piezoelectric laminates in cylindrical bending*, Int. J. Solids Struct., **32**, 2945–2960, 1995.
6. S.B. BEHESHTI-AVAL, M. LEZGY-NAZARGAH, *A finite element model for composite beams with piezoelectric layers using a sinus model*, J. Mech., **26**, 2, 249–258, 2010.
7. S.B. BEHESHTI-AVAL, M. LEZGY-NAZARGAH, *Assessment of velocity-acceleration feedback in optimal control of smart piezoelectric beams*, Smart Struct. Syst., **6**, 8, 921–938, 2010.
8. S.B. BEHESHTI-AVAL, M. LEZGY-NAZARGAH, P. VIDAL, O. POLIT, *A refined sinus finite element model for the analysis of piezoelectric laminated beams*, J. Intell. Mater. Syst. Struct., **22**, 203–219, 2011.
9. S.B. BEHESHTI-AVAL, M. LEZGY-NAZARGAH, *A coupled refined high-order global-local theory and finite element model for static electromechanical response of smart multilayered/sandwich beams*, Arch. Appl. Mech., **82**, 12, 1709–1752, 2012.

10. S.B. BEHESHTI-AVAL, M. LEZGY-NAZARGAH, *Coupled refined layerwise theory for dynamic free and forced response of piezoelectric laminated composite and sandwich beams*, *Meccanica*, **48**, 6, 1479–1500, 2013.
11. M. SHARIYAT, *Dynamic buckling of imperfect laminated plates with piezoelectric sensors and actuators subjected to thermo-electro-mechanical loadings, considering the temperature-dependency of the material properties*, *Compos. Struct.*, **88**, 228–239, 2009.
12. C. NIEZRECKI, D. BREI, S. BALAKRISHNAN, A. MOSKALIK, *Piezoelectric actuation: state of the art*, *Shock Vib. Dig.*, **33**, 4, 269–280, 2001.
13. X.H. ZHU, Z.Y. MENG, *Operational principle, fabrication and displacement characteristic of a functionally gradient piezoelectric ceramic actuator*, *Sens. Actuators, A*, **48**, 169–176, 1995.
14. C.C.M. WU, M. KAHN, W. MOY, *Piezoelectric ceramics with functional gradients: a new application in material design*, *J. Am. Ceram. Soc.*, **79**, 809–812, 1996.
15. G.R. LIU, J. TANI, *Surface waves in functionally gradient piezoelectric plates*, *ASME J. Vib. Acoust.*, **116**, 440–448, 1994.
16. W.Q. CHEN, H.J. DING, *On free vibration of a functionally graded piezoelectric rectangular plate*, *Acta Mech.*, **153**, 207–216, 2002.
17. H.J. LEE, *Layerwise laminate analysis of functionally graded piezoelectric bimorph beams*, *J. Intell Mater. Syst. Struct.*, **16**, 365–371, 2005.
18. Y. LI, Z. SHI, *Free vibration of a functionally graded piezoelectric beam via state-space based differential quadrature*, *Compos. Struct.*, **87**, 257–264, 2009.
19. J. YANG, H.J. XIANG, *Thermo-electro-mechanical characteristics of functionally graded piezoelectric actuators*, *Smart Mater. Struct.*, **16**, 784–797, 2007.
20. B. BEHJAT, M. SALEHI, M. SADIGHI, A. ARMIN, M. ABBASI, *Static, dynamic, and free vibration analysis of functionally graded piezoelectric panels using finite element method*, *J. Intell. Mater. Syst. Struct.*, **20**, 1635–1646, 2009.
21. B. BEHJAT, M. SALEHI, A. ARMIN, M. SADIGHI, M. ABBASI, *Static and dynamic analysis of functionally graded piezoelectric plates under mechanical and electrical loading*, *Scientia Iranica, Transactions B: Mech. Eng.*, **18**, 4, 986–994, 2011.
22. X.H. WU, C.Q. CHEN, Y.P. SHEN, *A high order theory for functionally graded piezoelectric shells*, *Int. J. Solids Struct.*, **39**, 5325–5344, 2002.
23. T. LI, Y.H. CHEN, J. MA, *Characterization of Fgm monomorph actuator fabricated using Epd*, *J. Mater. Sci.*, **40**, 3601–3605, 2005.
24. T.T. LIU, Z.F. SHI, *Bending behavior of functionally gradient piezoelectric cantilever*, *Ferroelectrics*, **308**, 43–51, 2004.
25. Z.F. SHI, Y. CHEN, *Functionally graded piezoelectric cantilever beam under load*, *Arch. Appl. Mech.*, **74**, 237–247, 2004.
26. H.J. XIANG, Z.F. SHI, *Static analysis for functionally graded piezoelectric actuators or sensors under a combined electro-thermal load*, *Eur. J. Mech. A Solids*, **28**, 338–346, 2009.
27. M. LEZGY-NAZARGAH, P. VIDAL, O. POLIT, *An efficient finite element model for static and dynamic analyses of functionally graded piezoelectric beams*, *Compos. Struct.*, **104**, 71–84, 2013.

28. M. LEZGY-NAZARGAH, M. FARAHBAKHS, *Optimum material gradient composition for the functionally graded piezoelectric beams*, Int. J. Eng. Sci. Tech., **5**, 4, 80–99, 2013.
29. S. BRISCHETTO, E. CARRERA, *Refined 2D models for the analysis of functionally graded piezoelectric plates*, J. Intell. Mater. Syst. Struct., **20**, 1783–1797, 2009.
30. C.W. LIM, L.H. HE, *Exact solution of a compositionally graded piezoelectric layer under uniform stretch, bending and twisting*, Int. J. Mech. Sci., **43**, 2479–2492, 2001.
31. J.N. REDDY, Z.Q. CHENG, *Three-dimensional solutions of smart functionally graded plates*, ASME J. Appl. Mech., **68**, 234–241, 2001.
32. Z. ZHONG, E.T. SHANG, *Three-dimensional exact analysis of a simply supported functionally gradient piezoelectric plate*, Int. J. Solids Struct., **40**, 5335–5352, 2003.
33. P. LU, H.P. LEE, C. LU, *An exact solution for functionally graded piezoelectric laminates in cylindrical bending*, Int. J. Mech. Sci., **47**, 437–458, 2005.
34. P. LU, H.P. LEE, C. LU, *Exact solutions for simply supported functionally graded piezoelectric laminates by Stroh-like formalism*, Comput. Struct., **72**, 352–363, 2006.
35. P. HEYLIGER, S. BROOKS, *Exact solutions for laminated piezoelectric plates in cylindrical bending*, J. Appl. Mech., **63**, 903–910, 1996.
36. F.R. GANTMAKHER, *The Theory of Matrices*, Chelsea, New York, 1959.
37. M.C. PEASE, *Methods of Matrix Algebra*, Academic Press, New York, 1965.
38. V.I. ALSHITS, H.O.K. KIRCHNER, *Elasticity of multilayers I. Basic equations and solutions*, Phil. Mag. A, **72** (6), 1431–1444, 1995.
39. V.I. ALSHITS, H.O.K. KIRCHNER, G.A. MAUGIN, *Elasticity of multilayers: properties of the propagator matrix and some applications*, Math. & Mech. Sol., **6**, 5, 481–502, 2001.
40. V.I. ALSHITS, G.A. MAUGIN, *Dynamics of multilayers: elastic waves in an anisotropic graded or stratified plate*, Wave Motion, **41**, 357–394, 2005.
41. A.L. SHUVALOV, O. PONCELET, M. DESCHAMPS, *General formalism for plane guided waves in transversely inhomogeneous anisotropic plates*, Wave Motion, **40**, 413–426, 2004.
42. A.L. SHUVALOV, O. PONCELET, A.P. KISELEV, *Shear horizontal waves in transversely inhomogeneous plates*, Wave Motion, **45**, 605–615, 2008.
43. J.P. NOWACKI, *Electro-elastic coupled fields of the general line source in infinite multilayered piezoelectric medium*, Arch. Mech. **64**, 1, 3–19, 2012.

Received March 9, 2014; revised version August 5, 2014.
